ChemPhysChem

Chemistry Europe
European Chemical Societies Publishing

Accepted Article

Title: Field Effect and Local Gating in Nitrogen-Terminated Nanopores (NtNP) and Nanogaps (NtNG) in Graphene

Authors: Ivana Djurišić, Miloš S. Dražić, Aleksandar Ž. Tomović, Marko Spasenović, Željko Šljivančanin, Vladimir P. Jovanović, and Radomir Zikic

To be cited as: *ChemPhysChem* 10.1002/cphc.202000771

Link to VoR: https://doi.org/10.1002/cphc.202000771

WILEY-VCH

ARTICLE WILEY-VCH

Field Effect and Local Gating in Nitrogen-Terminated Nanopores (NtNP) and Nanogaps (NtNG) in Graphene

Ivana Djurišić,[a] Miloš S. Dražić,[a] Aleksandar Ž. Tomović,[a] Marko Spasenović,[b] Željko Šljivančanin,[c] Vladimir P. Jovanović,[a] and Radomir Zikic*[a]

[a] I. Djurišić, Dr. M. S. Dražić, Dr. A. Ž. Tomović, Dr. V. P. Jovanović, Dr. R. Zikic
University of Belgrade, Institute for Multidisciplinary Research, Kneza Višeslava 1, 11030 Belgrade, Serbia
E-mail: radomir.zikic@sanu.ac.rs
[b] Dr. M. Spasenović
University of Belgrade, Institute of Chemistry, Technology and Metallurgy, Center of Microelectronic Technologies, Njegoševa 12, 11000 Belgrade, Serbia
[c] Dr. Ž. Šljivančanin
University of Belgrade, „Vinča" Institute of Nuclear Sciences - National Institute of the Republic of Serbia, PO Box 522, 11001 Belgrade, Serbia

Supporting information for this article is given via a link at the end of the document.

Abstract: Functionalization of electrodes is a wide-used strategy in various applications ranging from single-molecule sensing and protein sequencing, to ion trapping, to desalination. We demonstrate, employing DFT with Non-Equilibrium Green's Function formalism, that single-species (N, H, S, Cl, F) termination of graphene nanogap electrodes results in a strong in-gap electrostatic field, induced by species-dependent dipoles formed at the electrode ends. Consequently, the field increases or decreases electronic transport through a molecule (benzene) placed in the nanogap by shifting molecular levels by almost 2 eV in respect to the electrode Fermi level via a field effect akin to the one used for field-effect transistors. We also found the local gating in graphene nanopores terminated with different single-species atoms. Nitrogen-terminated nanogaps (NtNGs) and nanopores (NtNPs) result in the strongest effect. The in-gap potential can be transformed from a plateau-like to a saddle-like shape by tailoring NtNG and NtNP size and termination type. In particular, the saddle-like potential is applicable in single-ion trapping and desalination devices.

1. Introduction

Single-molecule sensing is important for detection or recognition of certain molecular species, as well as for the investigation of dynamics of chemical or biological processes, capturing rich single-molecule information rather than averaged ensemble properties [1, 2]. Sensors realized so far usually take advantage of intrinsic optical, electrical or mechanical molecular properties [1-3]. Electrical approaches offer some advantages such as fast, real-time label-free measurements, a high temporal resolution and potential for integration with silicon electronics. Single-molecule probing by tunneling currents, already applied to next-generation real-time single-molecule DNA and protein sequencing [4-6], is often a method of choice. Tunneling current is extremely sensitive to the position of a molecule placed in a nanogap between two nanoelectrodes and to its composition. Discrimination between molecules is based on variations of the tunneling current induced by the interaction of the molecule traversing the nanogap with the electrodes. The molecule-electrode interaction strongly depends on the choice of the electrodes [7, 8], which may or may not induce resonant transport through highest occupied/lowest unoccupied (HOMO/LUMO) molecular orbitals. Tunneling current may vary by several orders of magnitude depending on whether molecular levels participate in transport or not. Resonant transport is commonly accomplished by a careful selection of electrode termination species either for weak interaction between the molecule and electrodes (hydrogen bonding or Van der Waals interaction) [7, 9, 10] and/or for inducing an electrostatic field with electrode interface dipoles [11, 12].

Graphene is emerging as a particularly promising material not only for single-molecule probing [4, 5, 13-15], but for single-molecule electronics [11, 16, 17], single-atom magnets [18-20], energy storage [21] and nanofiltration [22-24] as well. It is atomically thin, planar material that can be utilized for transversal electrodes, and it is easily produced and integrated into devices [25]. Quite strikingly, and of utmost importance for electrical transport applications, tiny gaps with tunable dimensions have been made in graphene by nanostructuring [26] or piezoelectric positioning [27]. In molecular sampling applications, graphene edges are most commonly passivized (functionalized, terminated) with hydrogen atoms, however different terminations of graphene both simple (single-species passivation, with atomic nitrogen or hydrogen) [7, 28, 29] and more complex, with different recognition molecules [8, 10, 30] were used in order to achieve resonant transport. In nanofiltration applications, such as desalination, the type of termination of nanopores in graphene membranes, used as nanosieves, may determine what kind of ions are able to translocate the membrane [31].

Here, we found a strong field effect in graphene nanopores and nanogaps terminated with selected atomic species, systems well within experimental reach [27]. Employing DFT, the influence of *X*-terminated (*X* = N, H, F, S, Cl) semi-infinite graphene nanogap and nanopore on the position of the HOMO of a benzene molecule with respect to the Fermi energy E_F is shown to be determined by the shape and the strength of the in-gap electrostatic potential, raised as a consequence of termination-induced dipoles formed at the electrode edges. Furthermore, it is demonstrated that the potential generated by the dipoles approximated by linearly charged lines is in good agreement with DFT result, directly correlating the raising or lowering character of in-gap potential with dipole orientation. Dipole orientation is inherent property of termination specie-electrode interaction, influencing HOMO level shifting towards or away from the E_F. Finally, it was found that N termination is most prominent inducing the strongest field effect and shifting the HOMO level closest to E_F compared to other investigated species.

Computational Details

Calculations for empty nanogaps with different terminations and such gaps occupied by benzene molecules were performed using density functional theory (DFT) coupled with non-equilibrium Green's functions (NEGF) within the TranSIESTA package [32]. Positions of *X* (*X* = N, H, F, S, Cl) atoms that terminate graphene nanogaps are shown in Figure 1a. In-plane view of gap terminations is given in Supplementary Information (SI) Figure S1. The geometry of benzene molecules perpendicular (⊥) and parallel (∥) to the plane of the electrodes is given in Figures 1b,c, respectively. The central region, also called the scattering region or the extended molecule is marked with a dashed red rectangle (Figures 1b,c). Bulk electrodes are represented by six rows of carbon atoms. Geometries of N- and H-terminated graphene nanopores for TranSIESTA calculations are presented in Figures 1d,f, respectively, while corresponding geometries of pores with benzene are in Figures 1e,g, respectively. Both nanogap and nanopore systems are infinite in the *y* direction.

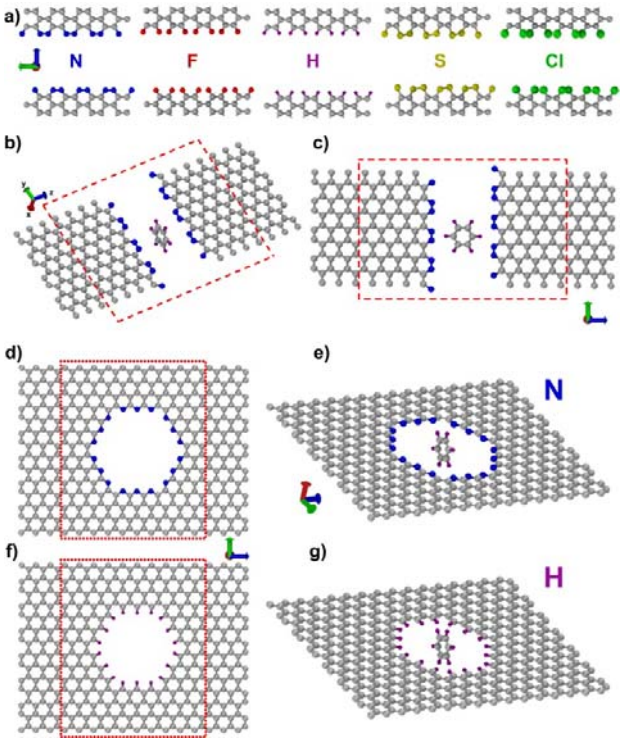

Figure 1. Optimized geometries used in TranSIESTA calculations of: a) empty *X*-terminated graphene gaps: *X* = N, H, F, S, Cl; N-terminated nanogap (NtNG) with a benzene molecule in b) perpendicular (⊥) and c) parallel (∥) orientations; d) empty N- and f) H-terminated graphene nanopores (NtNP and HtNP, respectively); e) NtNP and g) HtNP with benzene in perpendicular orientation. Dashed red lines mark the central region (the scattering region or the extended molecule), the size of which is the same for all terminations. Red, green, and blue arrows indicate *x*, *y*, and *z* directions, respectively.

Geometry optimization was performed using SIESTA [33]. First, the central regions of empty nanopores and nanogaps were optimized. The benzene molecule was then placed in the nanogap (parallel/perpendicular orientation) and nanopores (perpendicular orientation only), and finally the central region containing the molecule was optimized again. For the electrode and scattering region calculations in TranSIESTA, we used 1×9×64 and 1×9×1 k-points, respectively. For both SIESTA and TranSIESTA the basis set was double zeta polarized for all atoms, the exchange-correlation functional was approximated with the Perdew-Burke-Ernzerhof (PBE) functional [34], core electrons were described with Troullier-Martins norm-conserving pseudopotentials [35] and the mesh cutoff value was 170 Ry for the real-space grid. Charge excess per atom was obtained from Hirshfeld population analysis.

2. Results and Discussion

The edge functionalization effect on the electrostatic field was investigated by considered graphene nanogaps and nanopores with edges saturated by H, N, S, F, and Cl (Figure 1 and Figure S1 of the Supporting Information). For nanogaps we placed a benzene molecule in the middle of the gap and correlated the relevant molecular orbitals to the electrostatic field generated by the termination of graphene edges. Since the evolution of the electrostatic field with the type of the atomic species used to saturate the edges turns out to be the same for both (nanopore and nangap) graphene-based systems, the calculations for benzene at the nanopores was limited to N-terminated edges.

2.1 Field Effect in Empty Graphene Nanogaps

Geometries of optimized empty nanogaps are shown in Figure 1a (see also Figure S1). In the cases of N- and H-terminated nanogaps (NtNG and HtNG), the lowest energy structures have all atoms lying in the *y*-*z* plane, while for the other three cases (F, S, and Cl) termination and neighboring atoms are not confined to the graphene plane. The optimized structures for F and Cl terminations (Figure S1) are in accordance with previously reported results [36]. Placing a benzene molecule in the gap, both in parallel and perpendicular orientation do not significantly change the geometry of *X*-terminated gaps.

We calculate, from TranSIESTA, electrostatic potential energy E_p for *X*-terminated empty graphene gaps, the profiles of which along the midline parallel to the *z*-axis in the electrode plane are given in Figure 2a. The largest electrostatic potential energy in the center of the gap is obtained for N, followed by F, Cl, S and H termination. For F termination the value of E_p is almost zero (~20 meV). Compared to that value, the corresponding values of E_p for N and H terminations are shifted by +1.6 eV (upshift) and –0.7 eV (downshift).

The energy difference $E^{\perp}_{HOMO}(X)$, obtained from TranSIESTA, between the molecular HOMO (HOMO is not an orbital of an isolated molecule, it is rather a molecular projected self-consistent Hamiltonian HOMO) energy of benzene placed in a gap perpendicularly (Figure 1b) and the Fermi energy E_F depends on termination *X* (Figure 2b). The smallest $E^{\perp}_{HOMO}$ is obtained for N, followed by F, Cl, S and H termination. Again, compared to $E^{\perp}_{HOMO}$(F), there is an upshift by +1.4 eV and downshift by –0.6 eV of $E^{\perp}_{HOMO}$(N) and $E^{\perp}_{HOMO}$(H), respectively.

In the case of parallel orientation of benzene within a gap (Figure 1c), the variation of the difference $E^{\parallel}_{HOMO}$ between HOMO and Fermi energies with termination *X* is qualitatively the same as in the case of perpendicular orientation (Figure S2a). The benzene energy gap (~5.2 eV) is conserved in all calculations and it is sufficiently large to accommodate variations of $E^{\perp}_{HOMO}(X)$ and $E^{\parallel}_{HOMO}(X)$, the largest being for H termination (~2.6 eV).

Plotting center-of-the-gap $E_p(X) - E_p$(F) values and $E^{\perp}_{HOMO}(X) - E^{\perp}_{HOMO}$(F) on the same graph in Figure 2c implies that the dependence on termination species *X* of E_p and $E^{\perp}_{HOMO}$ is not just qualitatively, but also quantitatively almost the same. This is

valid for parallel orientation of benzene in the gap as well (Figure S2b). Thus, the variation of the molecular HOMO energy is primarily determined by the variation of the electrostatic potential of an empty gap with the termination species: we will define this as a *field-effect* similar to the one in solid-state electronics, with the difference that there is no gate electrode. However, nothing can be said *a priori* about the exact value of $E^{\perp}_{HOMO}(X)$.

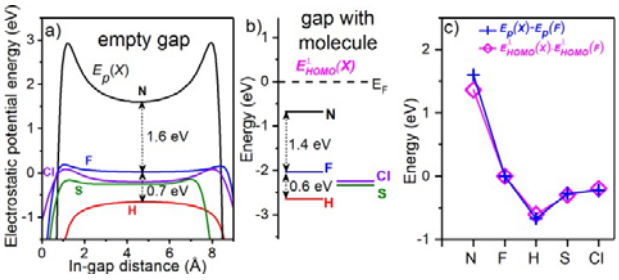

Figure 2. a) Electrostatic potential energy $E_p(X)$ of empty gap (Figure 1a) obtained by TranSIESTA along the midline parallel to the *z*-axis in the electrode plane for different terminations *X* (N – black, F – blue, Cl – violet, S – olive, and H – red). In-gap distance is measured from termination atoms on the left to the termination atoms on the right graphene sheet in the *z*-direction. b) The difference $E^{\perp}_{HOMO}(X)$ between the HOMO and the electrode Fermi energy for perpendicularly oriented benzene in *X*-terminated nanogaps (see Figure 1b). c) Center-of-the-gap $E_p(X)$ – E_p(F) values and $E^{\perp}_{HOMO}(X)$ – $E^{\perp}_{HOMO}$(F), represented with blue crosses and magenta diamonds, respectively.

We calculated in TranSIESTA transmission curves at zero bias for parallel orientation of benzene in the H- and N-terminated gaps (Figure S3a), to estimate their electrical currents in a zero-bias approximation. For N termination at a bias of 0.2 V, the current was estimated to 1.5 nA in the zero-bias approximation, while in the H-case, the current is at least five orders of magnitude smaller.

We have also performed TranSIESTA calculations of E_p for phosphorous termination of an empty gap as well, since N and P are in the same group in the periodic system. Unlike N, P atoms take out-of-plane positions in relaxed nanogap structures. The E_p profile along the midline parallel to the *z*-axis in the electrode plane is similar to H termination, with center-of-the-gap value of around -0.2 eV (Figure S3b). Although in the same family with nitrogen, phosphorous has no such strong field effect.

The dipole-induced field effect exists also in zigzag graphene nanogaps, based on our TranSIESTA calculations for their N and H functionalization (Figure S3c).

2.2 The Origin of the Field Effect

Using a simple model we will show that termination-dependent in-gap electrostatic potential energy and, consequently, the HOMO shift, originates from dipoles formed at the interfaces of graphene sheets (Figures 3a,b) [12]. From TranSIESTA Hirshfeld population analysis of NtNG, it can be seen that dipoles are formed by negative charge accumulated on the N termination atomic row and positive charge located on the adjacent row of C atoms (Figure 3a), while in the HtNG case, positive charge resides on H atoms while negative is located on the adjacent row of C atoms (Figure 3b). The presence of benzene in the gap does not significantly alter the charge distribution and dipole orientations in graphene (Figure S4).

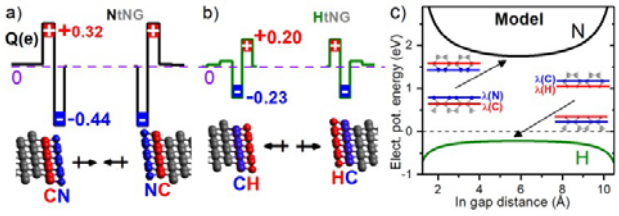

Figure 3. The sum *Q* of atomic Hirshfeld charge excesses for several rows of atoms in the *y*-direction of a) N- and b) H-terminated graphene nanogaps at zero bias (solid black line), obtained from TranSIESTA. Atomic rows bearing positive (negative) charge excess are colored red (blue). Arrows indicate the orientation of the dipoles formed by charge excesses of termination and adjacent rows of C atoms. c) Electrostatic potential energy (E_p) along the midline parallel to the *z*-axis in the electrode plane for NtNG (black line) and HtNG (green line) calculated from the four-line model. Inset: a model of four homogenously linearly charged lines represents corresponding rows of atoms (blue – negatively charged, red – positively charged) in graphene, whose total charge is equal to the one of the corresponding row. The length of the lines is ten times the length of the central region in the *y*-direction to approximate the infinity of graphene.

A simple model for the calculation of electrostatic potential energy consists of four homogeneously linearly charged lines lying in a single plane (inset of Figure 3c). The cases of N and H terminations for which E_p has minimal and maximal values are presented since their relaxed geometries are confined to the *y*-*z* plane, complying with the model. Each line represents one row of atoms (blue and red colors correspond to negative and positive charges, respectively) on graphene sheets. Linear charge densities λ(C) and $\lambda(X)$ were derived as total charge excess *Q* in one graphene row calculated from Hirshfeld analysis divided by the distance between the first and the last atom of that row. We have taken the length of the lines to be 10 times the length of the central region in the *y* direction to approximate the infinity of graphene. Calculated in-gap electrostatic potential energy along the midline parallel to the *z*-axis in the plane containing linear charges of N and H terminations is given in Figure 3c. Our model shows good qualitative agreement with the results obtained from TranSIESTA for an empty gap (Figure 2b). The simple model implies that the electrostatic potential energy calculated from TranSIESTA emanates from dipoles, i.e. that the local gating induced by properly chosen termination of the graphene sheet is the origin of the field effect.

Figure 3a shows that the charge is not equally distributed among N and adjacent C atomic rows, except for H termination (Figure 3b), for which the total charge of the dipole-forming lines is almost zero. We will distinguish two cases: a “symmetric” dipole (H termination) with $\lambda(X) = -\lambda(C)$ and an “asymmetric” dipole (N termination) with $\lambda(X) \neq -\lambda(C)$. The model implies that for the “symmetric” dipole, the field effect is stronger for a larger dipole moment (Figure S5a). Negative $\lambda(X)$ (solid lines in Figure S5a) produces positive electrostatic energy and a molecule placed in the nanogap would experience a positive shift of energy levels (Figure S5c). The opposite is true for $\lambda(X) > 0$ (dotted lines in Figure S5a). The “asymmetric” dipole is a more realistic description of *X*-terminated graphene. Electrostatic potential energy will be positive (negative) whenever the total charge $\lambda(X) + \lambda(C)$ of the dipole is negative (positive), irrespective of the orientation of the interface dipole (Figures S5b,c). The larger the total charge of the dipole (asymmetry), the larger the field effect (Figure S5c). The gap size and the distance (related to bond length) between dipole-forming lines can also influence the behavior of the energy but to a lesser extent.

2.3 Orientation of Benzene in the Nanogap

As seen, we placed the benzene molecule in the middle of *X*-terminated nanogaps in two different ways: in perpendicular and parallel orientations (Figure 1). In parallel orientation the spatial distance between the molecule and graphene gap edges is smaller than in the perpendicular case. Because of that the differences in optimized geometries of graphene sheets with and without benzene, though not pronounced, are larger in ∥ than in ⊥ orientation. Another effect of different orientations is manifested on the charge residing on the molecule. Figure S6 depicts charge excess *Q* of benzene in ⊥ and ∥ orientations in *X*-terminated graphene nanogaps obtained from TranSIESTA. For ⊥ orientation, $Q(X) \approx 0$, while for ∥ orientation charge excess is negative, except for H termination, for which $Q \approx 0$. Charge distribution at the nearest termination atoms is perturbed when the benzene molecule is introduced in the gap (Figure S7). For ⊥ orientation this perturbation is negligible, while it is notable for ∥ orientation, because of negative charge excess *Q* and reduced distance of benzene from gap edges. In accordance with References [17] and [37], we have previously shown [12] that even a small partial charge residing on the molecule in the gap (not in a weak coupling or quantum dot regime) can cause large energy shifts of molecular levels: negative charge on the molecule will result in positive energy shift of molecular energy levels [38]. Indeed, returning to Figure S2a, for ∥ orientation of benzene in the gap there is an upshift of HOMO energy compared to ⊥ orientation, $E^{\perp}_{HOMO}(X) < E^{\parallel}_{HOMO}(X)$, except for H termination, for which $E^{\perp}_{HOMO}(H) = E^{\parallel}_{HOMO}(H)$. For H termination $Q \approx 0$ in both ⊥ and ∥ cases, there is no charge redistribution between the molecule and the graphene (Figure S4), and, therefore, no energy shift of molecular levels for different molecular orientations. As shown in the previous subsections, the depth of HOMO below the Fermi level of benzene, no matter the orientation in the gap, will be primarily driven by the termination-dependent electrostatic potential energy of an empty gap (Figures 2 and S2). Thus, in the case the molecule placed in the gap does not interact (no charge redistribution on the molecule and termination atoms) with the *X*-terminated graphene sheets, the depth of the HOMO level below the Fermi energy will be determined only by local electrostatic potential energy induced by charges distributed on the edges of the gap.

2.4 Field Effect in Graphene Nanopores

In this section the field effect and local gating are demonstrated for another class of graphene-based systems within experimental reach – graphene nanopores. For empty graphene nanopores, various terminations, i.e. different charges (dipoles) at pore edges, induce different electrostatic potential energies, implying the existence of the field effect. As in the case of nanogaps, we will focus on N- and H-terminated graphene nanopores (NtNP and HtNP, Figure 1c). A TranSIESTA calculation gives saddle-shaped electrostatic potential energy E_p (Figure 4a). The electrostatic potential energy profiles for NtNP and HtNP are given in the left panel of Figure 4b. By analogy with results of calculations for nanogaps, the values of E_p in HtNP are lower than in NtNP, as expected. Additional tests of the structural and electronic properties of single-species terminated graphene nanopores have been performed using accurate GPAW code [39], based on the real space implementation of highly accurate projector augmented waves method [40, 41]. Excellent agreement with results produced with TranSIESTA program is presented in the Supplementary Information (Figures S8 and S9).

To demonstrate the field effect, the benzene molecule was placed (in the perpendicular orientation) in NtNP and HtNP (Figures 1e,g, respectively) and the difference E_{HOMO} between HOMO and Fermi energies was calculated in TranSIESTA (Figure 4b, right panel). Note that charge excess *Q* on benzene is zero. Center-of-the-gap $E_p(N) - E_p(H)$ and $E_{HOMO}(N) - E_{HOMO}(H)$ values are 1.7 and 2.0 eV, respectively (Figure 4b). The correlation between these two values clearly indicates a strong field effect, i.e. HOMO energy shift is driven by the electrostatic potential of empty nanopores. Its origin, in analogy with the nanogap case, is in charge distribution at the pore termination, as will be shown on the case of NtNP. As in the NtNG case, the charge distribution (obtained from Hirshfeld analysis in TranSIESTA) at termination N and next-neighbor C atoms of the NtNP (Figure 4c) is responsible for the saddle-shaped potential energy: N atoms bear negative, while next-neighbor C atoms carry a positive charge, forming a ring of radially oriented dipoles. Induced electron density for NtNP obtained using GPAW (Figure S10) supports the result of the Hirshfeld analysis. The saddle-shaped potential is also obtained from a model of two linearly charged rings (Figure 4d), which is in good qualitative agreement with TranSIESTA and GPAW calculations.

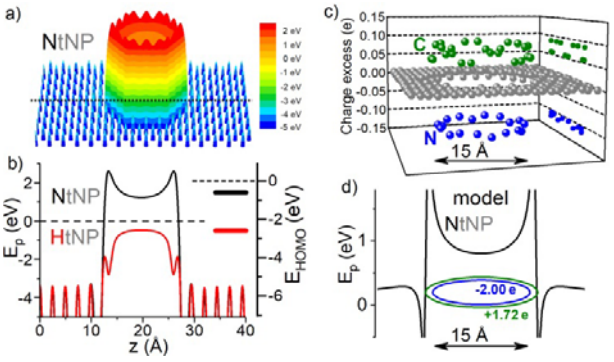

Figure 4. a) Electrostatic potential energy E_p in the *y*-*z* plane of empty nitrogen-terminated nanopore NtNP (see Figure 1d). b) Profiles of E_p (left panel) along the midline (dashed line in a) in the same plane for NtNP (black curve) and HtNP (red curve), whose optimized structures are in Figures 1d,f. The right panel shows $E_{HOMO}(N)$ (black) and $E_{HOMO}(H)$ (red) with respect to the corresponding electrode Fermi levels for benzene placed in N- and H-terminated graphene nanopores (their structures are in Figures 1e,g). c) Hirshfeld charge excess *q* for each atom in NtNP from Figure 1d: N atoms (blue balls), their next-neighboring C atoms (green balls), and other C atoms (grey balls). Projections of charge to the *x*-*z* plane are given for N and neighboring C atoms. d) Electrostatic potential energy profile obtained from two linearly charged rings along the axis defined by their perimeter. The total charge residing on each ring is equal to the corresponding net charge excess of N and C atoms from c.

3. Conclusion

In conclusion, we have shown that N termination of graphene nanogaps shifts the HOMO level of molecules within the gap closest to E_F when compared to F, H, S and Cl terminations.

This behavior is a consequence of an in-gap electrostatic field effect which arises from interface dipoles formed by graphene sheet termination. The in-gap field effect is also demonstrated for N-terminated graphene nanopores. From a practical standpoint, the local-gating field effect in NtNGs and NtNPs could improve the operation of single-molecule bio-sensing devices (primarily protein and DNA sequencing) based on transversal current by increasing electron transport several orders of magnitude. In applications with NtNPs one measures the in-plane current that is on the order of μA [15, 29]. The inclusion of molecular HOMO in transport only slightly affects in-plane current; however, such a small variation should be measurable due to its magnitude [15].

In addition, here shown graphene nanopores with saddle-shaped in-plane electrostatic potential have a potential to serve as a 2D matrix for novel functional materials. Being similar to graphene-embedded crown ethers that exhibit ion-trapping behavior, single-species-terminated nanopore arrays could be used as nanoscale strain sensors, strain-gated ionic transistors or nanofluidic logical devices [42]. Although the effects of pore terminations of graphene nanoporous membranes were studied before for water desalination [22, 23, 31], our results for the variation of the saddle-shaped potential with termination species, i.e. the charge at pore edges, could shed new light on membrane design in this field, as well as in the fields of gas separation [24] or nanopore-based protein and DNA sequencing [4, 6, 43, 44], even though benzene is smaller than the basic units of DNA or proteins, whose energy levels differ from those of benzene. For example, it would be expected that NtNPs and HtNPs would allow passage of different ions through membranes, and alternating the layers with N and H pore terminations would produce more efficient desalination of water.

Acknowledgements

This work was supported by the Ministry of Education, Science and Technological Development of the Republic of Serbia (Contract No. 451-03-68/2020-14/200053, 451-03-68/2020-14/200017, and 451-03-68/2020-14/200026). We gratefully acknowledge financial support from the Swiss National Science Foundation (SCOPES project No. 152406) and FP7-NMP, project acronym nanoDNAsequencing, GA214840.

Keywords: DFT+NEGF • field effect • graphene • sensors • termination

[1] J. Guan, C. Jia, Y. Li, Z. Liu, J. Wang, Z. Yang, C. Gu, D. Su, K. N. Houk, D. Zhang, X. Guo, *Sci. Adv.* **2018**, *4*, eaar2177.
[2] C. Gu, C. Jia, X. Guo, *Small Methods* **2017**, *1*, 1700071.
[3] J. J. Gooding, K. Gaus, *Angew. Chem. Int. Edit.* **2016**, *55*, 11354 – 11366.
[4] S. J. Heerema, C. Dekker, *Nat. Nanotechnol.* **2016**, *11*, 127–136.
[5] M. Di Ventra, M. Taniguchi, *Nat. Nanotechnol.* **2016**, *11*, 117–126.
[6] M. Graf, M. Lihter, D. Altus, S. Marion, A. Radenovic, *Nano Lett.* **2019** *19*, 9075-9083
[7] R. G. Amorim, A. R. Rocha, R. H. Scheicher, *J. Phys. Chem. C* **2016**, *120*, 19384−19388.
[8] J. Prasongkit, A. Grigoriev, B. Pathak, R. Ahuja, R. H. Scheicher, *J. Phys. Chem. C* **2013**, *117*, 15421–15428.
[9] V. Meunier, P. S. Krstić, *J. Chem. Phys.* **2008**, *128*, 041103.
[10] S. Biswas, S. Sen, J. O. Im, S. Biswas, P. Krstic, B. Ashcroft, C. Borges, Y. Zhao, S. Lindsay, P. Zhang, *ACS Nano* **2016**, *10*, 11304–11316.
[11] C. Van Dyck, V. Geskin, A. J. Kronemeijer, D. M. de Leeuw, J. Cornil, *Phys. Chem. Chem. Phys.* **2013**, *15*, 4392.
[12] I. Djurišić, M. S. Dražić, A. Ž. Tomović, M. Spasenović, Ž. Šljivančanin, V. P. Jovanović, R. Zikic, *ACS Appl. Nano Mater.* **2020**, *3*, 3034-3043.
[13] A. E. Rossini, F. Gala, M. Chinappi, G. Zollo, *Nanoscale* **2018**, *10*, 5928-5937.
[14] H. L. McFarland, T. Ahmed, J.-X. Zhu, A. V. Balatsky, J. T. Haraldsen, *J. Phys. Chem. Lett.* **2015**, *6*, 2616−2621.
[15] S. J. Heerema, L. Vicarelli, S. Pud, R. N. Schouten, H. W. Zandbergen, C. Dekker, *ACS Nano* **2018**, *12*, 2623-2633.
[16] N. Xin, J. Guan, C. Zhou, X. Chen, C. Gu, Y. Li, M. A. Ratner, A. Nitzan, J. F. Stoddart, X. Guo, *Nat. Rev. Phys.* **2019**, *1*, 211–230.
[17] A. Z. Thong, M. S. P. Shaffer, A. P. Horsfield, *Nanoscale* **2017**, *9*, 8119-8125
[18] F. Donati, S. Rusponi, S. Stepanow, C. Wäckerlin, A. Singha, L. Persichetti, R. Baltic, K. Diller, F. Patthey, E. Fernandes, J. Dreiser, Ž. Šljivančanin, K. Kummer, C. Nistor, P. Gambardella, H. Brune, *Science* **2016**, *352*, 318-321.
[19] F. D. Natterer, K. Yang, W. Paul, P. Willke, T. Choi, T. Greber, H. A. J., C. P. Lutz, *Nature* **2017**, *543*, 226–228.
[20] R. Baltic, M. Pivetta, F. Donati, C. Wa□ckerlin, A. Singha, J. Dreiser, S. Rusponi, H. Brune, *Nano Lett.* **2016**, *16*, 7610−7615.
[21] F. Zheng, Y. Yang, Q. Chen, *Nat. Commun.* **2014**, *5*, 5261.
[22] Y. Yang, X. Yang, L. Liang, Y. Gao, H. Cheng, X. Li, M. Zou, R. Ma, Q. Yuan, X. Duan, *Science* **2019**, *364*, 1057-1062.
[23] D. Cohen-Tanugi, J. C. Grossman, *Nano Lett.* **2012**, *12*, 3602−3608.
[24] A. W. Hauser, J. Schrier, P. Schwerdtfeger, *J. Phys. Chem. C* **2012**, *116*, 10819-10827.
[25] A. Zurutuza, C. Marinelli, *Nat. Nanotechnol.* **2014**, *9*, 730–734.
[26] O. Ochedowski, O. Lehtinen, U. Kaiser, A. Turchanin, B. Ban-d'Etat, H. Lebius, M. Karlušić, M. Jakšić, M. Schleberger, *Nanotechnology* **2015**, *26*, 465302.
[27] A. Bellunato, S. D. Vrbica, C. Sabater, E. W. de Vos, R. Fermin, K. N. Kanneworff, F. Galli, J. M. van Ruitenbeek, G. F. Schneider, *Nano Lett.* **2018**, *18*, 2505–2510.
[28] J. Prasongkit, A. Grigoriev, B. Pathak, R. Ahuja, R. H. Scheicher, *Nano Lett.* **2011**, *11*, 1941−1945.
[29] K. K. Saha, M. Drndić, B. K. Nikolić, *Nano Lett.* **2012**, *12*, 50–55.
[30] Y. Zhao, B. Ashcroft, P. Zhang, H. Liu, S. Sen, W. Song, J. O. Im, B. Gyarfas, S. Manna, S. Biswas, C. Borges, S. Lindsay, *Nat. Nanotechnol.* **2014**, *9*, 466–473.
[31] K. Sint, B. Wang, P. Král, *J. Am. Chem. Soc.* **2008**, *130*, 16448–16449.
[32] M. Brandbyge, J.-L. Mozos, P. Ordejón, J. Taylor, K. Stokbro, *Phys. Rev. B* **2002**, *65*, 165401.
[33] J. M. Soler, E. Artacho, J. D. Gale, A. García, J. Junquera, P. Ordejón, D. Sánchez-Portal, *J. Phys.-Condens. Mat.* **2002**, *14*, 2745–2779.
[34] J. P. Perdew, K. Burke, M. Ernzerhof, *Phys. Rev. Lett.* **1996**, *77*, 3865−3868.
[35] N. Troullier, J. L. Martins, *Phys. Rev. B* **1991**, *43*, 1993−2006.
[36] H. Jippo, M. Ohfuchi, *J. Appl. Phys.* **2013**, *113*, 183715.
[37] F. Zahid, A. W. Gosh, M. Paulsson, E. Polizzi, S. Datta, *Phys. Rev. B* **2004**, *70*, 245317-245321.
[38] M. Di Ventra, Electrical Transport in Nanoscale Systems, Cambridge University Press, Cambridge, **2008**.
[39] J. Enkovaara, C. Rostgaard, J. J. Mortensen, J. Chen, M. Dułak, L. Ferrighi, J. Gavnholt, C. Glinsvad, V. Haikola, H. A. Hansen, H. H. Kristoffersen, M. Kuisma, A. H. Larsen, L. Lehtovaara, M. Ljungberg, O. Lopez-Acevedo, P. G. Moses, J. Ojanen, T. Olsen, V. Petzold, N. A. Romero, J. Stausholm-Møller, M. Strange, G. A. Tritsaris, M. Vanin, M. Walter, B. Hammer, H. Häkkinen, G. K. H. Madsen, R. M. Nieminen, J. K. Nørskov, M. Puska, T. T. Rantala, J. Schiøtz, K. S. Thygesen, K. W. Jacobsen, *J. Phys.-Condens. Mat.* **2010**, *22*, 253202
[40] P. E. Blöchl, *Phys. Rev. B* **1994**, *50*, 17953.
[41] J. J. Mortensen, L. B. Hansen, K. W. Jacobsen, *Phys. Rev. B* **2005**, *71*, 035109.
[42] A. Fang, K. Kroenlein, D. Riccardi, S. A., *Nat. Mater.* **2019**, *18*, 76–81.
[43] S. Sahu, M. Zwolak, *Rev. Mod. Phys.* **2019**, *91*, 021004.
[44] L. Restrepo-Pérez, C. Joo, C. Dekker, *Nat. Nanotechnol.* **2018**, *13*, 786–796.